ISSN: 2639-0108

Research Article

Advances in Theoretical & Computational Physics

Thermal Simulation Analysis of a Lithium-Ion Battery

Jalaj Bidwai[1] and Pradip Majumdar[1*], David Schroeder[2] and S. Rao Kilaparti[2]

[1]*Department of Mechanical Engineering, Northern Illinois University, DeKalb, Illinois 60115*

[2]*Department of Technology, Northern Illinois University, DeKalb, Illinois 60115*

[*]Corresponding author
Pradip Majumdar, Department of Mechanical Engineering, Northern Illinois University, DeKalb, Illinois 60115, USA.

Submitted: 09 March 2021; **Accepted:** 15 March 2021; **Published:** 26 March 2021

Citation: *Jalaj Bidwai, Pradip Majumdar, David Schroeder, S. Rao Kilaparti (2021) Thermal Simulation Analysis of a Lithium-Ion Battery. Adv Theo Comp Phy 4(1): 82-93.*

Abstract

Lithium – Ion batteries are now extensively used in electric vehicles (EV) as well as in renewable power generation applications for both on-grid and off grid storage. Some of the major challenges with batteries for electric vehicles are the requirement of high energy density, compatibility with high charge and discharge rates while maintaining high performance, and prevention of any thermal runaway conditions. The objective of this research is to develop a computer simulation model for coupled electrochemical and thermal analysis and characterization of a lithium-ion battery performance subject to a range of charge and discharge loading, and thermal environmental conditions. The electrochemical model includes species and charge transport through the liquid and solid phases of electrode and electrolyte layers along with electrode kinetics. The thermal model includes several heat generation components such as reversible, irreversible and ohmic heating, and heat dissipation through layers of battery cell. Simulation is carried out to evaluate the electrochemical and thermal behavior with varying discharge rates. Results demonstrated a strong variation in the activation and ohmic polarization losses as well as in higher heat generation rates. Results show variation of different modes and order of cell heat generation rates that results in a higher rate of cell temperature rise as battery cell is subjected to higher discharge rates. The model developed will help in gaining a comprehensive insights of the complex transport processes in a cell and can form a platform for evaluating number new candidates for battery chemistry for enhanced battery performance and address safety issues associated with thermal runaway.

Keywords: Li-ion battery, Thermal Analysis, Multi physics Simulation

Introduction

Lithium – Ion batteries are now extensively used in electric vehicles (EV) as well as in renewable power generation applications for both on-grid-off grid storage. With the rapid decrease in the cost of battery storage, the EV vehicle market is undergoing an accelerated growth worldwide. Lithium-ion battery is the most popular candidates for EVs as well as for other energy storage applications because of its high energy density and extended life. For EV applications, the lithium-ion battery cells are subjected excessively high-power rates and variations during driving cycles. Under high charge and discharge rates and/or under extreme temperature environments, battery cells experience considerable degradation in the energy and power capacity of the cells [1-2]. As battery performance deteriorates due to increased polarization losses results in lower energy conversion efficiency and increased in heat generation. Inadequate control of such degradation effects and lack of efficient thermal management contributes to long term damages such as formation of solid-electrolyte interface (SEI) and dendrites formations, electrolyte decomposition leading towards thermal runway conditions [3]. While testing of battery cells or packs experimentally under controlled environment conditions give considerable understanding of the degradation of battery performance and rate of increase cell/pack temperatures [4-5], a more comprehensive understanding of the charge and heat transport rates, heat generation mechanisms, and conditions leading to thermal runway states of the battery can only be realized through computational simulation analysis [6].

Doyle et al. [7] used one-dimensional electrochemical model to study the performance of a lithium-ion battery cell made of LixC6 as a negative electrode and LiyMn2O4 as a positive electrode subjected to different discharge rates. The model included correlations for open-circuit voltage variations with state-of-charge. Pals and Newman [8, 9] integrated Doyle's electrochemical model developed by Doyle et al. [7] with a thermal model based on a global energy balance approach described by Bernardi et al. [10]. The model, however, neglected the local variation of temperature and its effects on transport process and electrode kinetics. T. I. Botte et al. [11] also used global energy approach to simulate the thermal behavior of the lithium-ion cell. Song and Evans [12] used a

two-dimensional thermal model that includes heat generation given by a one-dimensional electrochemical model.

Gu and Wang [13] developed a two-dimensional -D thermal and electrochemical coupled model for Li-ion battery with LixC6 as a negative electrode and LiyMn2O4 as a positive electrode. The model predicts the cell internal temperature distribution. Diffusion mass transfer resistance within the solid phase of the electrode particles is neglected. Cai and White [14] developed a one-dimensional model to estimate the surface temperature of the cell at various discharge rates and with different convective cooling conditions. Their 1D model included temperature and salt concentration dependent diffusion coefficient and the ionic conductivity in the binary electrolyte as suggested by Valoen and Reimers [15].

Srinivas and Wang [16] developed a two-dimensional assuming a linear dependency of surface concentration to the average concentration. The model incorporates reversible, irreversible and ohmic components of heat generation within the cell and includes the correlation data for e entropic reversible heat generation as a function of state-of-the- charge in the manganese oxide [17] battery cell. Their model shows the contribution of different types of heat generation with varying discharge rates. They have reported empirical correlation for the variation of the gradient of the op Al Hallaj et al. [18] reported data for dE/dT as a function of the voltage on the carbon negative electrode for estimating the state-of-charge using the correlation of the equilibrium potential vs. state-of-charge. These data obtained for the carbon negative electrode and the manganese oxide electrode are used by Venkat Srinivas and C.Y. Wang [16] in their study and are also used in the present study. The one-dimensional electrochemical model for Li-ion battery developed by Doyle et al. [7] has been implemented in the COMSOL [19] code as an analysis tool to study discharge behavior of the cell at different C-rates.

Subhedar et. al [20] performed combined electrochemical and thermal simulation analysis of battery configurations using multiphysics simulation code to understand the thermal management and cooling requirements of the batteries subject to the load cycle requirements of a locomotive engine. Primary goal of this study is to perform a feasibility analysis of modes of regenerating the energy developed in the braking and storing the energy in an electric battery storage system for use in road locomotive applications.

The objective of this research is to develop a computer simulation model for coupled electrochemical and thermal analysis for characterizing the lithium-ion battery performance over a range of charge and discharge loading, and thermal environmental conditions. The electrochemical model includes species and charge transport through the liquid and solid phases of electrode and electrolyte layers along with electrode kinetics. The thermal model includes several heat generation components such as reversible, irreversible and ohmic heating, and heat dissipation through layers of battery cell. The model developed will help in gaining a comprehensive insights of the complex processes and can form a platform for evaluating number new candidates for battery chemistry for enhanced battery performance and address thermal conditions that may lead to uncontrolled increasing high rate of heat generation, a phenomena known as the thermal runaway.

Battery Operation and Design

A battery cell converts chemical energy stored into electrical energy directly due to two spontaneous half reactions associated with two electrodes, separated by an electrolyte. During this process, the electrons transfer through external circuits performing electrical work as needed by the load.

During the discharge process the electrode which has low positive standard reduction potential undergoes an oxidation reaction producing positively charged Lithium ions and electrons. The positively charged Lithium ion migrate through the electrolyte towards, while electrons travel through external circuit towards the cathode electrode with higher standard reduction potential, which in turn undergoes a reduction reaction. During the charging of a rechargeable battery the reverse phenomenon happens; the Lithium ion move from the cathode electrode towards the anode electrode and the electrons are driven through external path towards the negative electrode.

Apart from the anode and cathode there are two other components required for the operation of the battery or a cell and they are electrolyte and the separator, which is a structural mesh partition that keeps the two electrodes physically separated and avoids short circuit. The electrolyte acts an insulator for the electrons and acts as conductor for Lithium ions to migrate between the electrodes.

Thermodynamic Open Circuit Voltage and Losses

Maximum possible voltage of an electrochemical cell is given by the thermodynamic reversible voltage as

$$-\frac{dG}{nF} = E^0 = -\frac{\Delta G}{nF}$$

The voltage obtained from this equation is the open circuit voltage, which is the voltage that is obtained from the battery when it is neither charging nor discharging, i.e., when no current is drawn or given to the cell. Cell operating voltage is reduced from the maximum possible voltage for a specific battery cell chemistry due to several polarization loss components. The polarization loss represents the deviation of the potential of the cell from the equilibrium potential when current is drawn from the cell. The typical performance polarization curve shown all major polarization losses is shown in Figure 1.

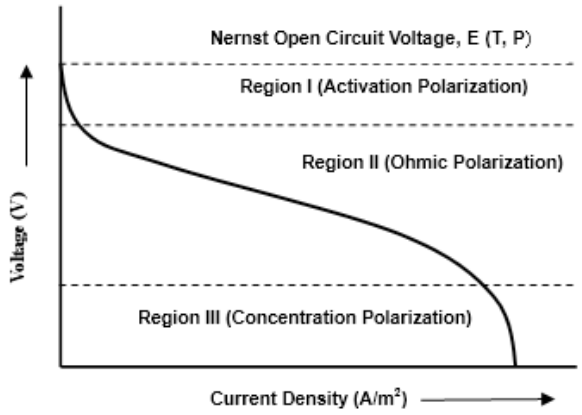

Figure 1: Various Losses associated with the Battery.

A brief description of the all types of polarization is explained as follows ***i. Activation Polarization (Region -I)*** is the voltage over potential loss is the energy expended in overcoming the barrier to electrochemical reactions at the electrode-electrolyte interface and this is prominent at lower current density. The expression for the activation polarization is derived from the electrode kinetics and given by the Butler-Volmer equation. Region I depict the activation polarization; ***ii. Ohmic Polarization (Region II)*** is the over potential caused by the resistance to the movement of the charged species like ions and electrons and this is predominant in moderate current densities; and ***iii Concentration Polarization (Region III)*** arises from the difference in the concentration of the reactants and the products at the electrode surface and in the bulk electrolytes. It is predominant at higher current densities.

Lithium-Ion Battery Cell Chemistry

Lithium-ion batteries are attractive because of their high specific energy and power density. Since lithium is one of the lightest metals, it is one of the most popular candidates for the search of the lower weight and smaller size battery storage systems for electric vehicles. Lithium is typically used as an intercalation material with carbon or graphite. Lithium ions during the discharging just get extracted from the structure of the carbon leaving the electron and during the charging they are inserted back. Other form anode materials that are currently being investigated are Silicone (Si) or composite mixture of Si and carbon or graphite or graphene.

A vast majority of the cathode materials that are being used or under development under study are primarily oxides of metals like Lithium Manganese Oxide(LMO), Lithium-Ion Phosphate (LFP or LIP), Lithium Cobalt Oxide (LCO)) and Lithium Nickel Oxide (NCO). In the present work Lithium Manganese Oxide ($LiyMn_2O_4$) is selected for the analysis as a cathode material. It has a good diffusion co-efficient as compared to the cobalt or nickel-based cathodes and does not release oxygen during overcharging. While this material has lower capacity than the cobalt and the nickel based cathodes, this along with Lithium Ion Phosphate ($LiyFeO_4$) are still the material of choice for any other application because it can be produced from less toxic materials, are less expensive material and have higher tolerance to thermal runway temperature conditions Most recently in EVs applications, alternate material composites are being considered, investigated and used to overcome the challenges associated increased cost of lithium and cobalt. Such materials include (NMC - Composites of Nickle-Manganese- Cobalt (NMC-111) or NMC-532.

Electrolytes are classified into three basic categories: liquid, solid and composite. Liquid electrolytes provide higher conductivity than solid electrolytes but are unstable chemically and require a porous separator to support them and thereby give them mechanical stability. One of the disadvantages of the liquid electrolyte is leakage and prone to the danger of thermal runway and safety failure.

Simulation Model

The lithium-ion battery model under consideration, shown in Figure 2, consists of a negative electrode current collector of copper (Cu), lithiated porous carbon as a ***negative electrode*** (Li_xC_6), lithiated porous manganese dioxide ($LiyMn_2O_4$) as a ***positive electrode***, positive electrode current collector of aluminum (Al) and a separator. The separator is a is a mesh made of a copolymer of vinylidene fluoride and hexafluoropropylene, (VdF-HFP). All the pores or the voids of the negative electrode, separator and the positive electrode are filled with electrolyte and forms the solution or the liquid phase of the cell. Electrolyte of the lithium-ion battery under consideration is a mixture of ethylene carbonate (EC-$C_3H_4O_3$) and dimethyl carbonate (DMC-$C_3H_6O_3$) with ***lithium hexafluorophosphate*** ($LiPF_6$) as the salt.

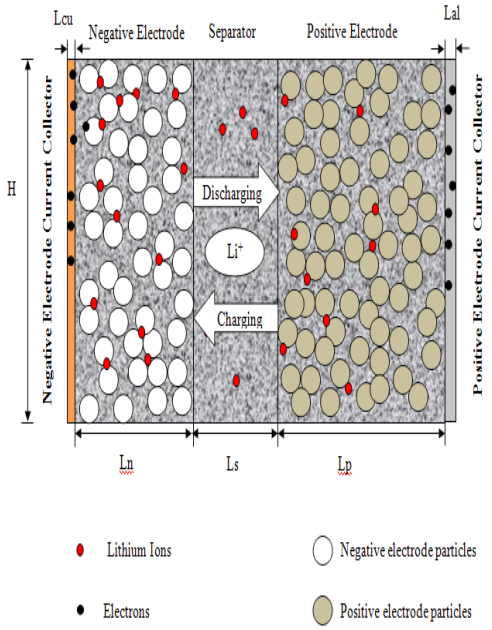

Figure 2: Schematic of a lithium-ion battery during charge and discharge

The de intercalation/intercalation reactions that occur during the charge and discharge process are shown below.

Reactions during discharge:

At the negative electrode (i.e., at anode)

$$Li_xC_6 \xrightarrow{\text{discharge}} xLi^+ + xe^- + 6C$$

and

At the positive electrode (i.e., at cathode)

$$xLi^+ + xe^- + Li_yMn_2O_4 \xrightarrow{\text{discharge}} Li_{x+y}Mn_2O_4$$

Reactions during charging:

At the negative electrode (i.e., at anode)

$$xLi^+ + xe^- + 6C \xrightarrow{\text{charge}} Li_xC_6$$

At the positive electrode (i.e., at cathode)

$$Li_{x+y}Mn_2O_4 \xrightarrow{\text{charge}} xLi^+ + xe^- + Li_yMn_2O_4$$

where x and y are the insertion factor for the negative and positive electrodes respectively and are defined as the ratio of the initial lithium concentration to the maximum concentration in the solid phase of the negative and positive electrode, respectively.

Modelling Approach

The two phases involving solid porous electrode and the liquid electrolyte are coupled by mass and charge balances, and the charge transfer reaction rates at the interfaces.

The following assumptions are taken into consideration while modeling the lithium-ion battery:1. No side reactions are neglected, 2. Transport of species in the electrolyte is through diffusion only, and convection is ignored, 3. The active electrode materials are made up of spherical particles with uniform size and constant porosity, 4. The ionic conductivity and the salt diffusion in electrolyte is assumed to functions of salt concentration and temperature, and 6. the effect of electric double layers and the film resistances are neglected.

Two different models are considered in this study to evaluate the sensitivity of the effects of temperature on some of the transport properties as well as its impact on the cell performance including heat dissipation rates. These models are described in the following section.

Temperature-independent (T-ID) electrochemical

In the temperature-independent electrochemical model the transport properties such as ionic conductivity of the binary electrolyte, diffusion co-efficient of the electrolyte and the solid-phase diffusion co-efficient are not considered as the function of temperature. The conductivity in this model is only considered to vary with electrolyte salt concentration. The empirical equation used is that given by Doyle et.al [7] and in a functional form of the ionic conductivity with the concentration shown as in Figure 3.

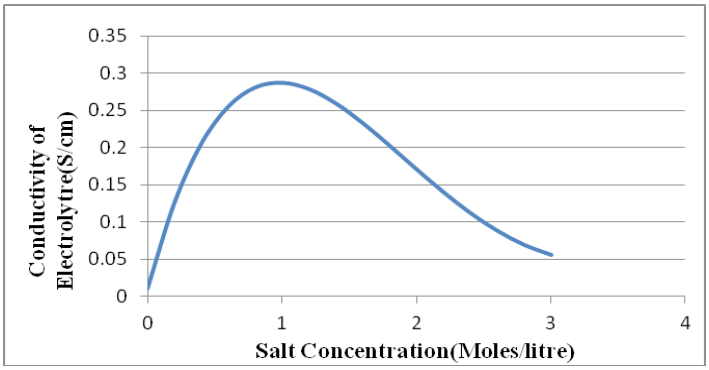

Figure 3: Conductivity of the LiPF6 in EC/DMC as a function of salt concentration

The variation shows that the ionic conductivity has a peak value of 0.28S/cm at a salt concentration of 1 moles/litre and decreases sharply as the concentration drops or increases from this peak value.

Temperature-Dependent (T-D) Electrochemical Model

In the temperature-dependent electrochemical model the above-transport properties are considered as a function of temperature. Ionic conductivity of the binary electrolyte and diffusion co-efficient in the electrolyte follows an empirical relation as reported by Valoen and Reimers [15].

The diffusion coefficient of salt in the electrolyte is given by

$$D_2 = 10^{-4} \times 10^{-4.43-\left(\frac{54}{T-229-5.0\times10^{-3}c}\right)-0.22\times10^{-3}c}$$

Where c is the concentration of the salt (moles/m3) and T is absolute temperature (K). The variation of the ionic conductivity and diffusion coefficient with the temperature and salt concentrations as given by the above two equations are depicted in Figure 4 and Figure 5. Data show strong dependence of ionic conductivity and the diffusion co-efficient in the temperature.

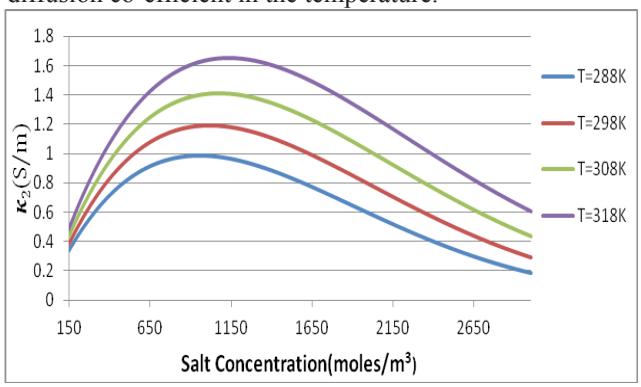

Figure 4: Ionic conductivity(S/m) of electrolyte as function of salt concentration and temperature

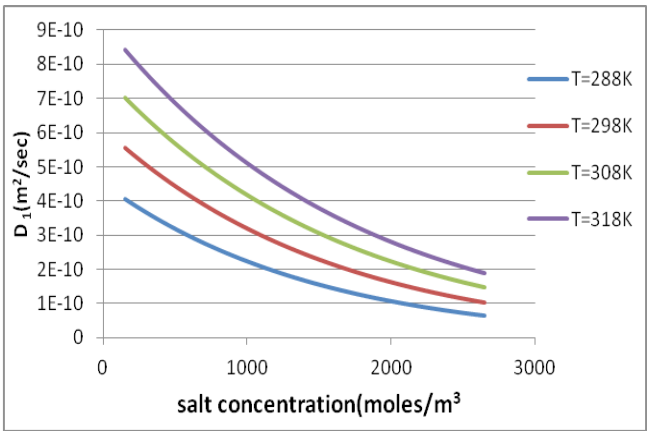

Figure 5: Diffusion Co-efficient of electrolyte as a function of salt concentration and temperature

Results show that the ionic conductivity of the electrolyte increases by 0.65 S/m as the temperature varies from 288K to 318K and the diffusion coefficient also sharply decreases with the electrolyte salt concentration. Arrhenius-type of equation is considered for incorporating the variation of the solid phase diffusion-coefficient with the temperature,

$$D_{l,k} = D_{ref,k}\left[\frac{E_{act}}{R}\left(\frac{1}{T_{ref}}-\frac{1}{T}\right)\right]$$

Where D_{lk} is the diffusion co-efficient in solid phase for electrode k, R is the universal gas constant, T_{ref} is the reference temperature, and E_{act} is the activation energy for the diffusion coefficient in the

solid phase. $D_{ref,k}$ is the diffusion coefficient in the solid phase at reference temperature.

Governing Equations

Conservation of charge and material balance equations along with the electrode kinetics equations are needed to describe the electrochemical phenomenon occurring in the battery. These equations are described for both solid and the liquid electrolyte phases.

Charge Balance

The charge valance equations represent the potential variations for the solid electrodes and electrolyte liquid phases.

Electronic Charge Balance in the Solid Phase

The charge balance equation governs the electronic current conduction in the solid matrix and solves for the potential in the solid phase of the electrode. This charge balance is expressed through Ohm's law given as

$$\nabla.\left(\sigma_k^{eff}.\nabla\Phi_{1,k}\right) = Q_1$$

where Q_1 is the source term given as

$$Q_1 = S_{a,k}FJ_{loc,k}$$

Combination of equation (9) and equation (10) leads to

$$\nabla.\left(\sigma_k^{eff}.\nabla\Phi_{1,k}\right) = S_{a,k}FJ_{loc,k}$$

where $\Phi_{1,k}$ is the potential in the solid phase of the electrode k and σ_k^{eff} is the effective electronic conductivity of the electrode material within the electrode k (k = n for the negative electrode or the anode and k = p for the positive electrode or the cathode) and is corrected using a Bruggeman correlation given by equation (11) below. S_a is the specific surface area (m^2/m^3). is the pore-wall flux determined by the electrode kinetics or the Butler-Volmer equation and F is Faraday's constant (96485 Col/Moles).

$$\sigma_k^{eff} = \sigma_k\varepsilon_k{}^{brug}$$

Where σ_k is the electronic conductivity of the solid phase of region k, ***brug*** is the Bruggeman co-efficient and is taken as 1.5 [7] and is the solid phase porosity of electrodes. The index k is n for the negative electrode and p for the positive electrode.

Ionic Charge Balance in Liquid Phase

Charge balance in the liquid phase is expressed by the modified Ohm's Law as given by,

$$\nabla.\left[\left(-\kappa_2^{eff}\nabla\Phi_2 + \frac{\kappa_2^{eff}RT}{F}\left\{1+\frac{d\ln f}{d\ln c}\right\}(1-t_+^0).\nabla\ln c\right)\right] = Q_2$$

where Q_2 is the charge source term given as

$$Q_2 = S_{a,k}FJ_{loc,k}$$

Combination of equation (12) and equation (13) leads to,

$$\nabla.\left[\left(-\kappa_2^{eff}\nabla\Phi_2 + \frac{\kappa_2^{eff}RT}{F}\left\{1+\frac{d\ln f}{d\ln c}\right\}(1-t_+^0).\nabla\ln c\right)\right] = S_{a,k}FJ_{loc,k}$$

Where k_2^{eff} (S/m) is the effective ionic conductivity of the electrolyte.

The solution phase ionic conductivity is corrected by taking porosity and tortuosity factor into account and is given by,

$$\kappa_2^{eff} = \kappa_2\varepsilon_k{}^{\gamma}$$

Where k_2 is the conductivity of the electrolyte and is a function of electrolyte salt concentration.

Material Balance

Material balance equations govern the concentration of the lithium in the solid and the liquid phase.

Material Balance in Solid Phase

The material balance in the solid phase is done by assuming a single particle model. The electrodes are assumed to consist of such spherical intercalation particles with identical size and shape. The mass balance of the lithium in the intercalation particle of the electrode active material is given by Fick's second law in a spherical co-ordinate system.

$$\frac{\partial c_{1,k}}{\partial t} = D_{1,k}\frac{1}{r^2}\frac{\partial}{\partial r}\left[r^2\frac{\partial c_{1,k}}{\partial r}\right]$$

Where $c_{1,k}$ is the solid phase lithium concentration and $D_{1,k}$ is the solid phase diffusion co-efficient of lithium ions in the electrode, and k is the index representing the negative and the positive electrodes (k is n for the negative electrode and p for the positive electrode).

Boundary conditions:

At the center of the spherical particle

$$-D_{1,k}\frac{\partial c_{1,k}}{\partial r} = 0 \text{ at } r = 0$$

On the surface of the particle the flux is equal to the consumption/production rate of Li ions due to the electrochemical reaction occurring at the solid/liquid interface.

$$-D_{1,k}\frac{\partial c_{1,k}}{\partial r} = j_{loc,k} \qquad \text{at } r = R_{1,k}$$

Material Balance in the Liquid Phase

The material balance for the lithium ion in the liquid phase is given by,

$$\varepsilon_k\frac{\partial c}{\partial t} = \nabla.\left(D_2^{eff}\nabla c\right) + (1-t_+^0)S_{a,k}j_{loc,k}$$

Where ε_k is the porosity of the region k (k is **n** for the negative electrode, **p** for the positive electrode and **s** for the separator). D_2^{eff} is the diffusion co-efficient of the salt in the solution phase and c ($moles/m^3$) is the electrolyte salt concentration.Sa, k is the specific area of electrode k, jloc, k is the pore wall flux given by electrode kinetics and t^0_+ is the cationic transference number.

Electrode Kinetics

The charge transfer reaction is assumed to occur at the interface of the solid and the electrolyte or the liquid phase. The rate of the intercalation/de intercalation reactions is given by the Butler-Volmer Kinetics equation. This relation is based on the difference between the cathodic and anodic currents and is given by,

$$j_{loc,k} = \frac{i_{0,k}}{F}\left[\exp\left(\frac{\alpha_{a,k}F\eta_{s,k}}{RT}\right) - \exp\left(\frac{\alpha_{c,k}F\eta_{s,k}}{RT}\right)\right]$$

Where $i_{0,k}$ is the exchange current density and is given as

$$i_{0,k} = k_k c^{\alpha_{a,k}} \left(c_{s,max,k} - c_{s,k}\right)^{\alpha_{a,k}} c_{s,k}^{\alpha_{c,k}}$$

Where $\alpha_{a,k}$ is the anodic charge transfer co-efficient for the electrode reaction, $\alpha_{a,k}$ is the cathodic charge transfer coefficient for the electrode reaction $\eta_{s,k}$ is the surface over potential of the electrode reaction given by

$$\eta_{s,k} = \Phi_{1,k} - \Phi_{2,k} - E_k$$

The term Ek is the open-circuit potential of the electrode k and it varies with the state of the charge (SOC). The experimental correlations of the open circuit potential as a function of SOC for both the electrodes are given by Doyle *et al.* [7]. The curve-fitted correlation of the open circuit potential as a function of the state-of-the-charge (x = SOC) for the carbon electrode is given as,

$$E_n = -0.16 + 1.32\exp(-3.0x) + 10.0\exp(-2000.0x)$$

Where **x** is given by the ratio of the initial lithium concentration in the negative electrode and the maximum concentration in the solid phase of the negative electrode and is given as,

$$x = \frac{c_{l,n}^0}{c_{l,n}^{max}}$$

Where $c^0_{l,n}$ and c_{ln}^{max} are the initial and maximum lithium concentration in the solid phase of the negative electrode.

The variation of the open circuit potential with the state-of-the-charge (SOC) for the carbon electrode is depicted in Figure 6.

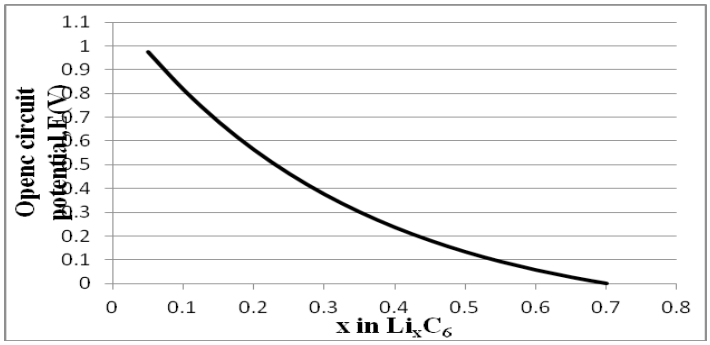

Figure 6: Open-circuit potential of LixC6 as a function of SOC.

The open-circuit potential variation with the state-of-the- charge (y = SOC) for the manganese dioxide cathode electrode is given as

$$E_p = 4.19829 + 0.0565661\tanh(-4.5546y + 8.60942) - 0.275479\left[\frac{1}{(0.998432 - y)^{0.492465}} - 1.90111\right] - 0.157123\exp(-0.04738y) + 0.810239\exp[-40(y - 0.133875)]$$

Where **y** is given by the ratio of the initial lithium concentration in the positive electrode and the maximum concentration in the solid phase of the positive electrode and is given as,

$$y = \frac{c_{l,p}^0}{c_{l,p}^{max}}$$

where $c^0_{l,p}$ and $c^{max}_{l,p}$ are the initial and maximum lithium concentration in the solid phase of the positive electrode. A plot for the open circuit potential vs state of charge for the manganese dioxide electrode is shown in Figure 7. The variation shows a sharp drop in potential near as concentration approaches unity.

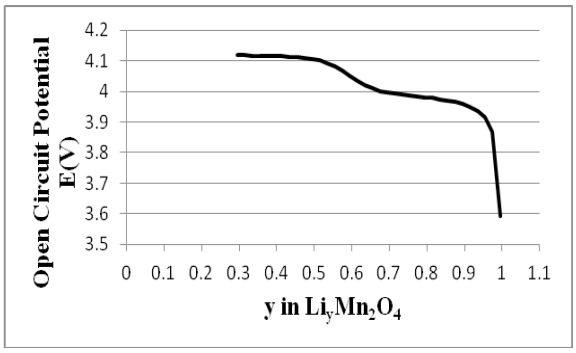

Figure 7: Open Circuit Potential of LMO as a function of SOC

Initial and Boundary Conditions for the Electrochemical Model
All the initial and boundary conditions used for the electrochemical model are discussed in the following section.

Initial Conditions

Uniform initial conditions are specified for T, c and c1, k at time t=0

a) The temperature of the cell is specified as,

$$T = T^0$$

b) The initial electrolyte concentration is,

$$C = C^0$$

c) The solid phase lithium concentration for negative electrode is,

$$c_{l,n} = c_{l,n}^0$$

d) The solid phase lithium concentration for the positive electrode is,

$$c_{1,p} = c_{1,p}^0$$

Boundary Conditions for the Charge balance in the Solid Phase

a) On the copper current collector tab, the potential in the solid phase is set to zero.

$$\Phi_{l,k} = 0$$

b) While on the aluminium current collector tab, the solid phase current density is equated to the applied current density and expressed as

$$-\sigma_k^{eff}\frac{\partial \Phi_{l,k}}{\partial n} = I_{app}$$

where I_{app} is the applied current density (A/m^2).

c) While at all other boundaries, current in the solid phase is assumed insulated and expressed as

$$-\sigma_k^{eff}\frac{\partial \Phi_{l,k}}{\partial n} = 0$$

Boundary Conditions for the Charge balance in the liquid/electrolyte Phase

a. At the interfaces of the electrodes and the separator the potential in the solution phase i.e., and its fluxes are continuous.
b. At the outer boundaries, there is no charge flux in the liquid phase and expressed as,

$$-\sigma_k^{eff}\frac{\partial \Phi_{2,k}}{\partial n}=0$$

Boundary Conditions for the material balance in the liquid/electrolyte phase

The concentration of the binary electrolyte and its fluxes are continuous at the interface between the negative electrode/separator and the separator/positive electrode. At the outer boundaries, there is no mass flux and expressed as,

$$-k_k^{eff}\frac{\partial c}{\partial n}=0$$

Thermal Analysis Model

The he thermal behavior of the battery during the charge/discharge load cycle is analyzed considering couple energy balance equation along with the electrochemical model. Objective is to gain considerable insight analysis on different forms and variation of the heat generation term during charge/discharge cycle. The heat transport equation is given as,

$$\frac{\partial\left(\rho_k c_{p,k} T\right)}{\partial t}=\nabla.\left(\lambda_k \nabla T\right)+q$$

Where k is n for the negative electrode, p for the positive electrode and s for the separator, $C_{P,K}$ is the average specific heat conductivity of porous region, ρ_K is the density of porous region, and λ_k is the average thermal conductivity of region. The ***second term*** on the right-hand side, q is the heat generation term, and is composed of three major components: i) reaction heat generation due deviation of battery potential from equilibrium potential termed as ***irreversible heat generation, ii) reversible heat generation*** due to the entropic effect, and iii) ***Ohmic heating*** due to charge transport through the electrodes, electrolytes, and current collector plates. The total heat generation term is given as,

$$q=j_{loc,k}.\left(\Phi_{1,k}-\Phi_{2,k}-E_k\right)+j_{loc,k}.T\frac{dE_k}{dT}+\sigma_k^{eff}\nabla\Phi_{1,k}.\nabla\Phi_{1,k}$$
$$+\kappa_2^{eff}\nabla\Phi_{2,k}.\nabla\Phi_{2,k}+\kappa_D^{eff}\nabla \ln c.\nabla\Phi_{2,k}$$

The coefficient k^{eff}_D in the above expression is

$$\kappa_D^{eff}=\frac{\kappa_2^{eff}RT}{F}\left\{1+\frac{d\ln f}{d\ln c}\right\}\left(1-t_+^0\right)$$

Where $\Phi_{1,k}$ and $\Phi_{1,k}$ is the potential in the solid and the liquid phase in region k respectively (k is n for negative electrode and p for positive electrode). j_{lock} is the pore-wall flux of Li^+ in the electrode k and is given by the Butler – Volmer Kinetics and E_K is the open circuit potential of the electrode k with respect to a lithium reference electrode.

The first term in the right-hand side of equation (38) gives the deviation of the potential from the equilibrium potential and is termed as reversible heat; the second term arises from reversible heat generation. The rest of the terms represents ohmic heating. The reversible heat generation relation is used based on the data for the LMO as reported by Thomas *et al* [11]. This data was curve-fitted in to the empirical relation, and the plot of the expression is shown in Figure 8. It shows that in a range of SOC or y-values from approximately 0.45 to 0.60 and after approximately 0.75, d(Ep)/dT values becomes negative. As the reversible heat is a function of d(Ep)/dT, it is apparent that the reaction becomes endothermic and consumes energy for y-values in the range of 0.45 - 0.60.

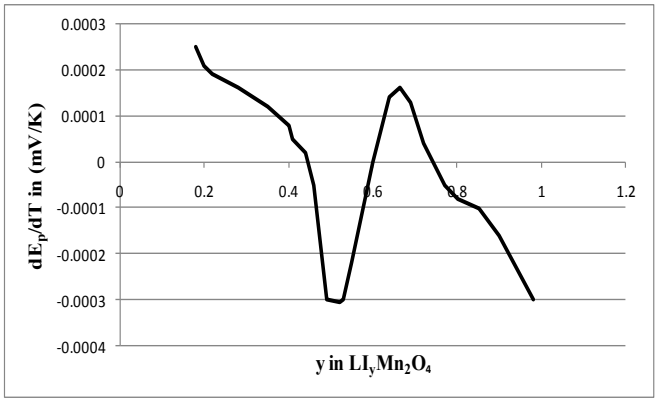

Figure 8: Variation of equilibrium potential with respect to temperature to the SOC for LMO.

For the lithiated carbon electrode, Al Hallaj *et al* [12] reported experimental data on the variation of the open circuit voltage with temperature. Doyle *et al* [1] used this data set and obtained the correlation for the variation of the open circuit potential with SOC as a is depicted in the Figure 9.

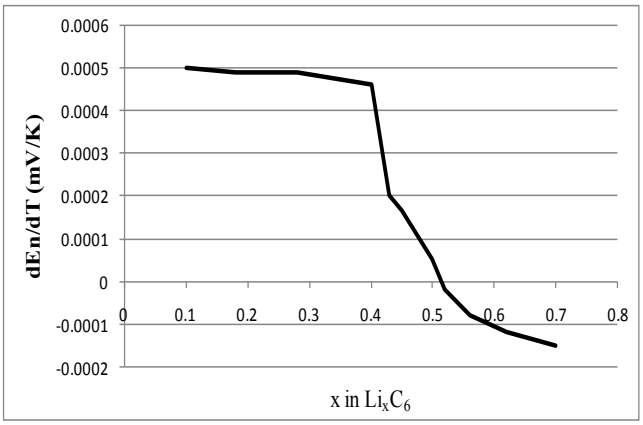

Figure 9: Variation of Equilibrium potential gradient with respect to the SOC for the lithiated carbon. electrode.

Results and Discussions

Simulations are performed using COMSOL commercial code to analyze the performance of a Li-ion battery under different charge/discharge load cycles and thermal environments.

To understand the sensitivity of temperature on the species transport properties and heat dissipation rates, simulations are carried out using temperature-dependent (T-D) and temperature-independent (T-ID) model. Figures 10 and 11 shows the cell potential vari-

ation and average cell temperature with time for the T-D model and T-ID model for the cell discharged rate of at 2C- rate considering adiabatic boundary conditions maintained at the bottom and at the sides, and convective cooling from the top. Adiabatic boundary conditions are given to see the variation in the temperature and cell potential when the cell is completely isolated from the surroundings.

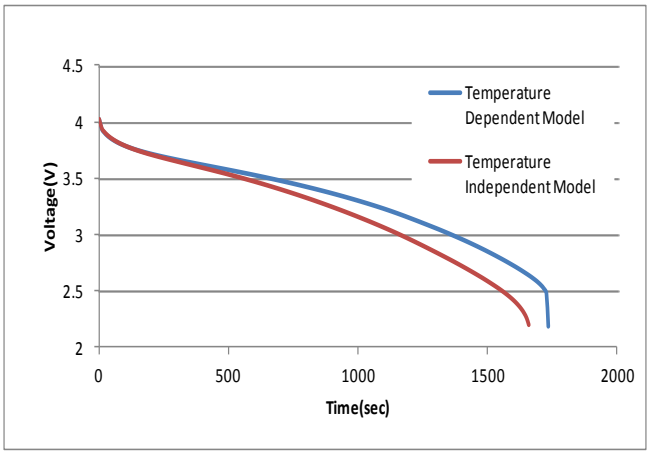

Figure 10: Cell potential for the coupled and decoupled model at 2C-discharge rate

The cell potential curve shows that there is increased ohmic loss in the T-ID model S COMPRED TO THE T-D model as the discharge progresses, and hence there is increased the voltage drop. It is evident that that T-ID model increasingly under-predicts the cell potential during discharge with increasing time.

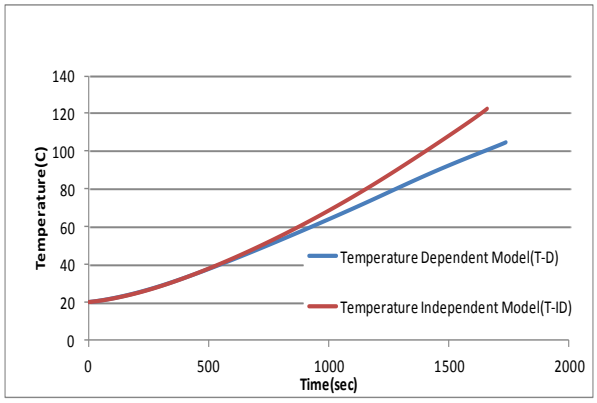

Figure 11: Average Cell Temperature for T-D and T-ID model at a 2C discharge rate.

It can be seen the Figure 11 that the average cell temperature predicted by the T-ID model is significantly higher than that given by the T-D model. At the end of the discharge time, the T-D model predicts the temperature approximately 104°C as compared to the cell temperature of 122°C predicted by the T-ID model.

The contour plots and the line plots in Figure 12 and 13 respectively show the temperature variation in the cell for models.

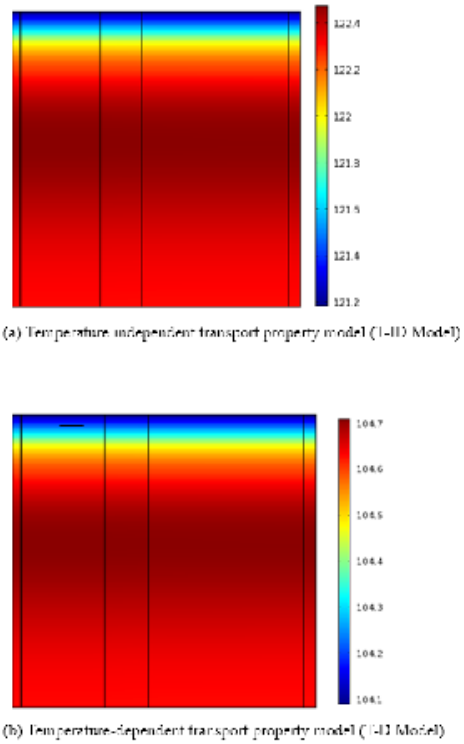

Figure 12: Contour Plots for cell temperature (^{O}C) variation using (a) T-ID model and (b)T-D model

Results in Figure 12 show a higher temperature level near the mid-section of the cell with a gradual drop in temperature towards the top surface due to diffusion of heat in the cell and convective cooling from the top surface.

Figure 13 shows a line plot of temperature variation along a vertical line from the bottom surface to the top surface at the mid-section. While both T-ID model and T-D model show peak temperature near the mid-height of the battery, the T-ID model shows a significantly higher peak value nearer to the top surface. For T-D model the cell temperature reaches to only 104°C, while for the T-ID model it reaches around 122°C, which is 18°C higher in T-ID model than T-D model. Moreover, the temperature drops quickly along the cell height for the T-D model. At 0.3 m height the cell temperature is 122.4964 °C for the T-ID model which is 17.77% higher than T-D model.

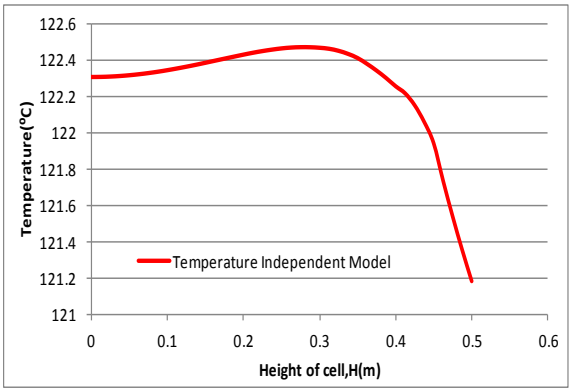

(a) T-ID model

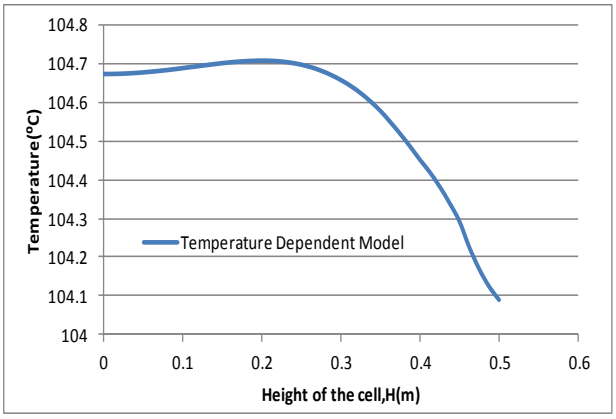

(a) T-ID model

Figure 13: Temperature along the height (H=50cm) of the cell. (a) T-ID model (b) T-D model

This difference in the lower cell temperature and higher cell potential is due to better mass diffusion for the T-D model than T-ID model. The mass diffusivity of the ions increases with temperature and which in turn helps in facilitating easy ion transport. The concentration profiles for the temperature-independent and temperature-dependent model at height h=0.25m, from the bottom is shown in the Figure 14.

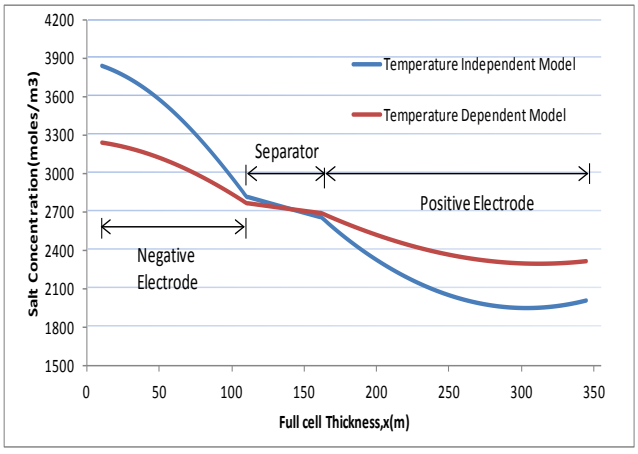

Figure 14: Concentration profile at h=0.5m from the bottom for T-D and T-ID model

From the above plot the concentration profile for the T-D model show more uniform spatial variation across the cell compared to the steeper variation given by the T-ID model. This is due to the enhanced diffusion of the species in the T-D model.

This shows the importance of incorporating temperature-dependent transport properties. It can be concluded that the T-ID model may give rise to a high error in predicting the cell performance in terms of polarization losses, heat generation and cell temperature rise, and therefore the T-D model is essential for further performance analysis of the lithium-ion cell.

Analysis at Different C-Rates

As C-rate represents the rate at which the battery is charged or discharged, the battery SOC decreases at sharper rates as the C-rate is increased, severely effecting the capacity as well as on the mass species transport and heat generation, heat transport and thermal state of the battery. The average cell temperature and the surface temperature of the cell also depend upon the C-rate and therefore to see the effect of the variation of the C-rate on the cell performance this analysis is of utmost importance. In this analysis, the thermal model includes convective boundary conditions with the convective heat transfer-coefficient on the top and on the sides, while the bottom is assumed as adiabatic.

Figure 15 shows the cell potential drop during discharge at different C-rates. Results demonstrate that the battery voltage at a sharper rate for higher C-rates i and hence greatly affects the energy storage capacity of the battery. The plots indicate increase in activation polarization and ohmic polarization losses with increased discharge rates. At higher discharge rate, i.e., at 4C, the concentration loss is not seen. Voltage dropped from 4.2V to 2.8V in around 600 seconds for 4C rate compared to near 3400 seconds for 1C rate.

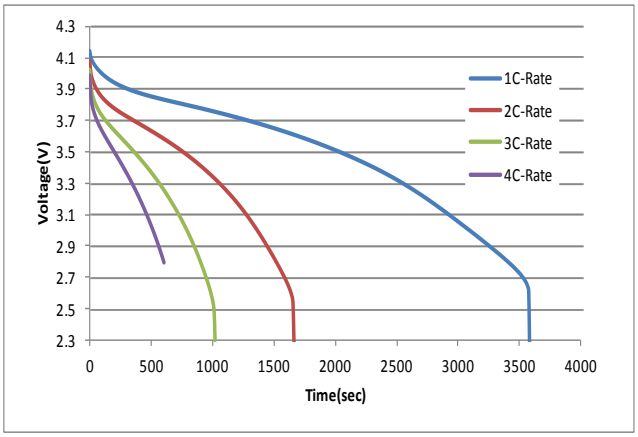

Figure 15: Cell Potential at different Discharge Rates

Contribution of different components of heat

Figure 16 indicates the effects of increasing C-rates on heat generation. The contribution of the different components of heat generation such as reversible, irreversible and the ohmic components of heat generation for different C-rates are plotted in Figure 16.

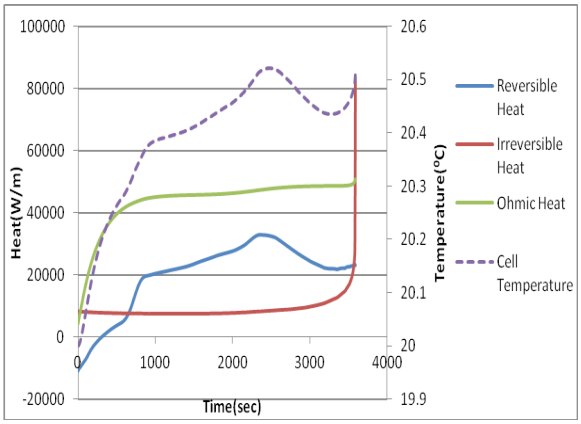

(a) 1C-rate

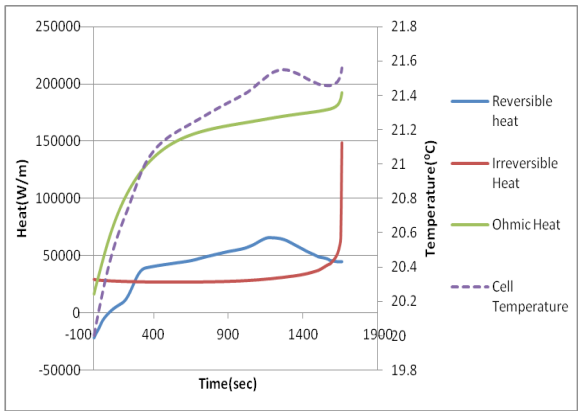

(b) 2C-rate

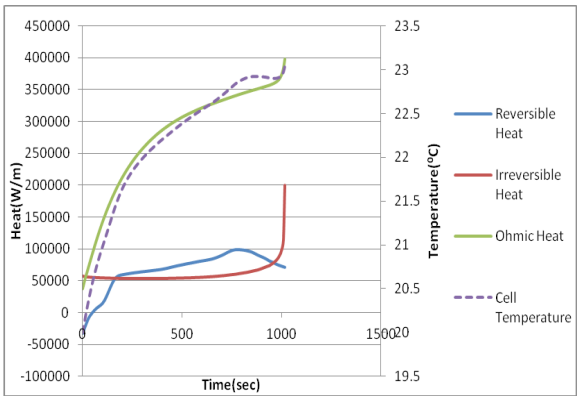

(c) 3C-rate

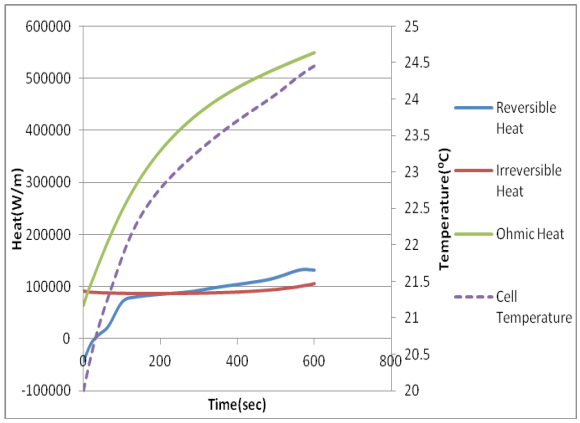

(d) 4C-rate

Figure 16: Contribution of all heats and cell temperature. (a) 1C-Rate (b) 2C-Rate (c) 3C-Rate (d) 4C-Rate

Figure 16 depicts some interesting phenomena occurring in the cell. The noteworthy effect of increasing the C-rate on the contribution of different components of heat generation can be seen. Irreversible and ohmic heats are exothermic (i.e., heat releasing) for all the C-rates and its effect is on the increase of temperature during the discharge. The ohmic heat continuously increases as the discharge proceeds and increases with C-rate increment. The irreversible heat generation, on the other hand, also increases with the C-rate and at the end of discharge rates for 1C, 2C and 3C rates. The irreversible heat generation as represented by equation (37) is a function of $(\Phi_{1,K}-\Phi_{2,K}-E_k)$ which also represents the concentration loss. This heat goes up suddenly to an exceedingly high value at the end of discharge due to the prominence of the concentration loss, which can be seen in the cell potential curve in Figure 15. For 4C-rate, the concentration loss is not seen and that is why the sudden increase of the irreversible heat is not seen for this discharge rate.

The reversible heat plays a particularly important role, as this is the only component of heat which goes negative during the discharge process. This endothermic (i.e., heat-consuming) effect of reversible heat has a significant effect on the temperature variation in the cell. The nature of the reversible heat curve is dictated by the dE/dT vs SOC curve. At the beginning of the discharge this heat is negative due to the negative values of dE/dT (i.e., 0.00008mV/K at initial SOC of 0.56 for negative electrode). AS s the discharge proceeds, this value becomes positive and so is the reversible heat generation.

The reversible heat generation plays a significant role in the lithium-ion cell even at a high discharge rate, but when the discharge rate is decreased the effect of reversible heat is further manifested. To see the effect of reversible heat at low discharge rate, a simulation run is performed by specifying a discharge rate of 0.1C. Figure 17 points out to some interesting facts. At a low discharge (0.1C), i.e., when the cell is at near equilibrium, the importance of reversible heat is seen. Under these conditions most of the temperature rise takes place due to reversible heat generation and it can be seen from the proximity of the reversible heat generation line with the total heat generation line.

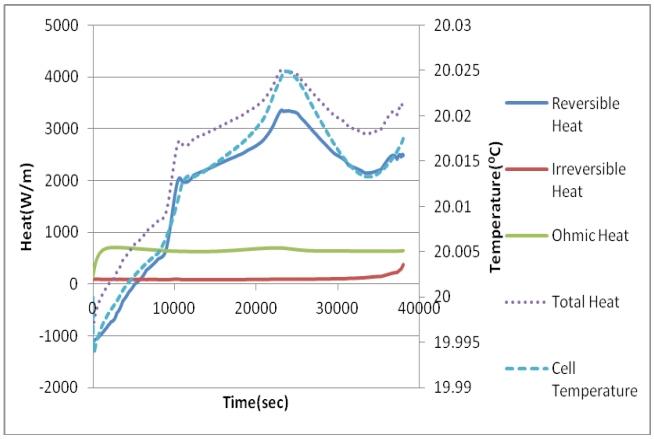

Figure 17: Heat contribution and cell temperature at 0.1C

Figure 18 shows an increase in cell temperature with the increase in C-rate. The maximum cell temperature for 4C discharge is 24.45°C, which is approximately 19.1 % higher than the maximum temperature reached for 1C rate. Moreover, maximum temperature 4C rate is reached at the end of the discharge while for 1C-rate this temperature is reached approximately 69% depth-of-discharge. Increasing C-rate has a significant on the cell temperature and these calls for the need of a proper thermal management system for the battery storage system.

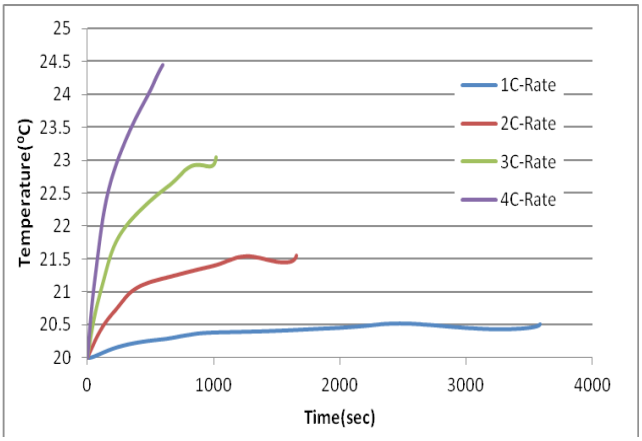

Figure 18: Cell Temperature at different C-Rates

Conclusions

A multi-dimensional and Multi physics model is presented to analyze lithium-ion battery cell to demonstrate the effects of number of key elements such as the temperature dependent transport properties, and charge/discharge rates on the cell polarization performance, degree and nature of heat generations and temperature rise and the rates of heat dissipations. Simulation results show sensitivity of discharge rates on the electrochemical performance and thermal conditions of the battery. Variation in the voltage loss due to reaction; different form of heat generations and dominant ohmic polarization with increase in discharge rates. The cell temperature distributions for increased discharge rates indicate the need for cooling of the cell to control and suppress the higher rate of temperature rise to avoid any potential uncontrolled reactions and failure of the battery cell components that may lead to thermal runaway control, and an identify needs for a proper control scheme for discharge rates and cooling scheme. The model developed helps in gaining a good insights of the complex processes and can form a platform for evaluation other candidate battery chemistries in identifying materials for enhanced battery performance and thermal management system for EVs and renewable energy storage applications. Such an analysis assists in addressing the key issue of operating the battery at a maximum efficiency level while dissipating any excessive heat generated during the operation and maintaining the battery at a desired temperature range using a cooling scheme.

Acknowledgment

The work is supported by U.S. Department o work is supported by U.S. Department of Energy under Grant No: DE-EE0003975.

References

1. EV Thomas, I Bloom, JP Christophersen, VS Battaglia (2012) Rate-based degradation modeling of lithium-ion cells, Journal of Power Sources 206: 378-382.
2. CR Birkl, MR Roberts, E McTurk, PG Bruce and DA Howey (2017) Degradation diagnostics for lithium-ion cells, Journal of Power Sources 341: 373-386.
3. JR Belt, CD Ho, CG Motloch, TJ Miller, and TQ Duong (2003) A Capacity and power fade study of Li-ion cells during life cycle testing, Journal of Power Sources 123: 241-246.
4. Andrew Arendas, Pradip Majumdar, S Rao Kilaparti and David Schroeder (2013) Experimental Investigation of the Thermal Characteristics of Li-Ion Battery for Use in Hybrid Locomotives, ASME Journal of Thermal Science and Engineering Application.
5. Krishnashis Chatterjee, Pradip Majumdar, David Schroeder and S Rao Kilaparti (2018) Performance Analysis of Li-ion Battery Under Various Thermal Load Conditions, ASME Journal of Electrochemical Energy Conversion and Storage 16(2).
6. J Harlow, X Ma, J Lai, E Logan, Y Liu, et al. (2019) A Wide Range of Testing Results on an Excellent Lithium-Ion Cell Chemistry to be used as Benchmarks for New Battery Technologies, Journal of Electrochemical Society 166: A3031-A3044.
7. M Doyle, J Newman, AS Gozdz, CN Schmitz, and J Tarascon (1996) "Comparison of Modeling Predictions with Experimental Data from Plastic Lithium-Ion Cells", Journal of Electrochemical Society 143: 1890.
8. C Pals and J Newman (1995) "Thermal Modeling of the Lithium/Polymer Battery", Journal of Electrochemical Society 142: 3274.
9. C Pals and J Newman (1995) "Thermal Modeling of the Lithium/Polymer Battery", Journal of electrochemical society 142: 3282.
10. D Bernardi, E Pawlikowski, and J Newman (1985) "A General Energy Balance for Battery Systems", Journal of Electrochemical Society 132: 5.
11. G Botte, B Johnson, and R White (1999) "Influence of Some Design Variables on the Thermal Behaviour of a Lithium-Ion Cell", Journal of Electrochemical Society 146: 914.
12. L Song and JW Evans (2000) "Electrochemical-Thermal Model of Lithium Polymer Batteries", Journal of Electrochemical Society 147: 2086.
13. WB Gu and CY Wang (2000) "Thermal-Electrochemical Coupled Modelling of a Lithium-Ion Cell", Journal of Electrochemical Society 147: 2910-2922.
14. Long Cai and Ralph E White (2011) "Mathematical modelling of a lithium-ion battery with thermal effects on COMSOL Inc. Multi physics (MP) software", Journal of Power Sources 196: 5985-5989.
15. Lars Ole Valoen and Jan Reimers (2005) "Transport Properties of LiPF6-Based Li-Ion Battery Electrolytes", Journal of Electrochemical Society 152: A882-A891.
16. Venkat Srinivasan and CY Wang (2003) "Analysis of Electrochemical and thermal Behaviour of Li-ion Cells", Journal of Electrochemical Society 150: A98-A106.
17. K Thomas, C Boguta, and J Newman (2001) "Measurement of the Entropy of Reaction as a Function of State of Charge in Doped and Undoped Lithium Manganese Oxide", Journal of Electrochemical Society 148: A570.
18. S Al Hallaj, R Venkatachalapathy, J Prakash, and JR Selman (2000) "Entropy Changes Due to Structural Transformation in the Graphite Anode and Phase Change of the LiCoO2 Cathode", Journal of Electrochemical Society 147: 2432.

19. COMSOL 4.1(a) Documentation.
20. Sarang Subhedar, Pradip Majumdar, David Schroeder and Rao Kilaparti (2017) Thermal Simulation Analysis of Battery Storage System for Hybrid Locomotive, Journal of Multidisciplinary Engineering Science Studies 3: 1940-1949.